Arabian Journal of Chemistry (2017) **10**, 1039–1051

King Saud University

Arabian Journal of Chemistry

www.ksu.edu.sa
www.sciencedirect.com

ORIGINAL ARTICLE

Triazole containing magnetic core-silica shell nanoparticles for Pb^{2+}, Cu^{2+} and Zn^{2+} removal

Zakaria Mokadem [a], Sofiane Mekki [a], Salima Saïdi-Besbes [a,*], Geraldine Agusti [b], Abdelhamid Elaissari [b], Aicha Derdour [a]

[a] *University Oran 1 Ahmed Benbella, Laboratoire de Synthèse Organique Appliquée (LSOA), Département de chimie, Faculté des sciences exactes et appliquées, BP 1524 EL Mnaouer, 31000 Oran, Algeria*
[b] *University Lyon-1, Villeurbanne, CNRS, UMR-5007, LAGEP-CPE, 43 bd 11 Novembre 1918, F-69622 Villeurbanne, France*

Received 1 August 2016; revised 11 December 2016; accepted 11 December 2016
Available online 24 December 2016

KEYWORDS

Magnetic;
Nanoparticles;
Triazole;
Adsorption;
Desorption;
Heavy metal ions

Abstract The main goal of this work was to investigate the ability of 1,2,3-triazole functionalized magnetic nanoparticles (MNP-Trz) and silica coated MNP homologous (MNPS-Trz) for removal of heavy metal cations. Three steps for efficient synthetic pathway were used for chemical modification of magnetic core based on copper catalyzed 1,3-dipolar cycloaddition. The magnetic nanoparticles were characterized by using various techniques such as X-ray diffraction (WAXD), infrared spectroscopy (FTIR), thermogravimetry analysis (TGA), zeta potential analysis, transmission electron microscopy (TEM) and scanning electron microscopy (SEM). The adsorption of prepared nanosized magnetic nanoparticles toward Cu^{2+}, Pb^{2+} and Zn^{2+} ions was examined as a function of various physical-chemistry conditions. Adsorption isotherms and kinetics were studied and discussed by considering various theoretical models. The equilibrium kinetics was found to be second order model irrespective of investigated system. The best corroborating model with the obtained experimental results was found to be Langmuir one with maximum adsorption capacities at pH 5.5 and 25 °C for Cu^{2+}, Pb^{2+} and Zn^{2+} ions found to be 87.87, 167.78 and 51.20 mg g^{-1}, respectively. Similar high maximum uptake tendency was also obtained for magnetic core-silica shell nanoparticles. It is interesting to notice that the regeneration of the used MNP-Trz was successfully achieved by using 0.1 M HNO_3 since 88% desorption efficiency was reached.

1. Introduction

Heavy metal ions are the most significant source of water and soil pollution. This contamination is usually associated with intensive industry activities, mining smelting and agricultural (Duruibe et al., 2007; Khan et al., 2008; Albarracín-Sánchez et al., 2013). Roadways and automobiles are also considered to be one of the largest sources of heavy metals. Zinc, copper, lead, nickel and cadmium are usually found in road

* Corresponding author. Fax: +213 41513077.
E-mail addresses: salima_saidi@yahoo.fr, saidi.salima@univ-oran.dz (S. Saïdi-Besbes).
Peer review under responsibility of King Saud University.

Production and hosting by Elsevier

http://dx.doi.org/10.1016/j.arabjc.2016.12.008
1878-5352

runoff and exhaust. The persistence of heavy metals in wastewaters is due to their non-biodegradable nature and their tendency to accumulate in the living organisms causing various diseases and disorders.

Different approaches for heavy metal removal from wastewaters have been used. These include various physical, chemical and biological methods such as chemical precipitation (Broomberg et al., 1999), liquid–liquid extraction (Ambashta and Sillanpää, 2010), ion-exchange (Mahdavian and Mirrahimi, 2010), adsorption (Zhang et al., 2013), filtration (Fu and Wang, 2011; Ozaki et al., 2002), electrochemical treatment (Chen, 2004), membrane technologies (Chen et al., 2009), biomaterials and polymeric ligand chelators (Samiey et al., 2014).

Adsorption method was extensively studied for metal removal because it is easy to perform, relatively low-cost and effective process. Various adsorbent materials have been used including clay (Potgieter et al., 2006), polysaccharides (Zhou et al., 2004; Crini, 2005), carbon nanotubes (Chen et al., 2009), zeolites (Oliveira et al., 2004) and functionalized polymers (Rether and Schuster, 2003; Ge et al., 2012). The adsorption efficiency of heavy metals is mainly adsorbent chemical nature and is closely tied to the accessibility of metal ions to active sites (Chen, 2004). After complexation of metal ions, the separation and regeneration of adsorbents was not always obvious. Filtration steps using energy-intensive pumping to speed the filtration process are often required. Thus, considerable efforts have been done for tailoring novel adsorbent materials exhibiting selective, fast complexation of metal ions and reusability for several times for metals removal from aqueous media.

Recently, magnetic dispersions and particularly iron oxide based particles are gaining increasing attention for wastewater treatments (Ray and Shipley, 2015; Xu et al., 2012). They exhibit interesting specific properties in comparison with the corresponding bulk material. In fact, they show high specific surface to volume ratio, low sedimentation due to low size, easy to prepare, low coast, good biocompatibility and low toxicity (Badruddoza et al., 2010). Magnetic particles have also the advantage to be superparamagnetic and could be easily collected and removed with an external magnetic field without any chemical degradation of the active sites.

Nowadays, a wide range of iron-based functionalized materials find application in the removal of heavy ions either by exchange or by sorption or chemical reaction (Broomberg et al., 1999). For specific ion separation, functional groups are immobilized to magnetic substrates through vapor condensation, polymer coating, surfactant adsorption or direct silylation with silane coupling agents (Ambashta and Sillanpää, 2010; Mahdavian and Mirrahimi, 2010). For this purpose, magnetite and maghemite nanoparticles functionalized with different active synthons such as amine (Hao et al., 2010), phosphonic acids (Mohapatra and Pramanik, 2009), carboxylic acid (Mohapatra et al., 2007), dimercaptosuccinic acid (Yantasee et al., 2007) groups and natural or synthetic polymers such as chitosan (Tran et al., 2010), alginate (Ngomsik et al., 2009), β-cyclodextrin (Badruddoza et al., 2011), poly (acrylic acid) (Mahdavian and Mirrahimi, 2010; Huang and Chen, 2009) and gum Arabic (Banerjee and Chen, 2007) have been recently reported in the literature.

In the last decades, the five-membered aromatic nitrogen heterocycles have attracted particular interest as ligands due to their ability to act as polydentate ligands since they contain potentially two, three or four nitrogen-donor atoms. Among such versatile heterocycles used for the preparation of coordination materials, 1,2,3-triazole structural unit is gaining more and more importance (Obata et al., 2008). It combines multiple interesting properties including a high chemical and thermal stabilities, a strong dipole moment, an aromatic character and a good hydrogen-bond-accepting ability (Zhang et al., 2006; Tome, 2004). The great revival experienced in the synthesis of [1,2,3]-triazole compounds in the form of the copper catalyzed Huisgen cycloaddition allows for the obtention of various functionalized triazole derivatives in a versatile way and led to renewed interest in the coordination chemistry of the 1,4-functionalized 1,2,3-triazoles (Juríček et al., 2011). A range of new mono, bi, tri and polydentate 1,2,3-triazole containing ligand architectures have been synthesized and their coordination properties examined (Crowley and Bandeen, 2009). We recently demonstrated that poly(1,2,3-triazole) colloidal particles could adsorb efficiently Cu^{2+}, Co^{2+} and Ni^{2+} ions and that the stability of the metal complexes increased with the metal ion charge/radius ratio in the following order $Cu^{2+} > Ni^{2+} > Co^{2+}$ (Lahmar et al., 2015).

The aim of this work was to design and characterization of novel Fe_3O_4-based magnetic nanoparticles modified with 1,2,3-triazole unit (MNP-Trz) and their silica-coated homologous (MNPS-Trz). The use of a silica protective shell will enhance the chemical stability of particles in acid media particularly during the regeneration process, prevents their aggregation in solution and reduces their toxicity. Their adsorption behavior of three heavy metal ions Cu^{2+}, Zn^{2+} and Pb^{2+} was investigated and compared. The effect of various parameters was studied such as pH, incubation time and initial metal concentrations in order to understand the mechanism of prepared magnetic particles to adsorb and to remove investigated metal ions. A synergistic effect between magnetite and triazole hetrocycle was confirmed that affects positively the adsorption behavior of MNP-Trz adsorbent in comparison with the crude iron oxide material.

2. Material and methods

2.1. Materials

Ferric chloride hexahydrate ($FeCl_3{\cdot}6H_2O$, 98%), Ferrous chloride tetrahydrate ($FeCl_2{\cdot}4H_2O$, 99%), 3-aminopropyltriethoxysilane ($H_2N(CH_2)_3Si(OC_2H_5)_3$, APTES, >99%), Tetraethylortho silicate ($Si(OC_2H_5)_4$, TEOS > 99%), 1, N, N′-dicyclohexylcarbodiimide (DCC), 4-dimethylaminopyridine (DMAP), propargyl acid, sodium ascorbate, copper sulfate pentahydrate ($CuSO_4{\cdot}5H_2O$), sodium hydroxide (NaOH, >98%), and hydrochloric acid (37%) were purchased from Sigma-Aldrich (Prochima Sigma, Tlemcen, Algeria).

The solvents were of commercial grade quality and were dried and distilled before use. Ethanol HPLC grade (99%), dichloromethane (DCM, 99%) and tert-Butanol (⩾99.0%) were purchased from Sigma-Aldrich (Prochima Sigma, Tlemcen, Algeria). Toluene (99%) was obtained from Biochem, Algiers.

$CuCl_2{\cdot}4H_2O$, $Pb(NO_3)_2$, $Zn(NO_3)_2{\cdot}4H_2O$ were purchased from Sigma-Aldrich (Prochima Sigma, Tlemcen, Algeria) and were used as source of Cu(II), Pb(II) and Zn(II) ions. Deionized water was used for all experiments.

4-azido-1-nitrobenzene was prepared according to Nolting and Michel method (Noelting and Michel, 1893) with a yield of 79%.

2.2. Preparation of magnetite (Fe_3O_4)

The magnetite nanoparticles (MNP) were prepared by the conventional co-precipitation method corresponding to the following reaction path:

$$2FeCl_3 + FeCl_2 + 8NH_3 + 4H_2O \rightarrow Fe_3O_4 + 8NH_4Cl \quad (1)$$

$FeCl_3{\cdot}6H_2O$ (11.68 g) and $FeCl_2{\cdot}4H_2O$ (4.30 g) were dissolved in 200 mL of deionized water under nitrogen atmosphere with vigorous stirring. The pH of the solution is increased by adding dropwise 12.5 mL of NH_4OH solution (28%) into the above mixture under continuous stirring. The color of the solution turned black immediately. The reaction mixture was heated at 80 °C for 2 h at 300 rpm. After cooling

the suspension to room temperature, the resulting Fe_3O_4 nanoparticles were separated using a magnet and then washed with deionized water to remove the base excess until the pH becomes neutral. The black precipitate was then washed three times with ethanol (3 × 50 mL) and dried in vacuum.

2.3. Functionalization of magnetic nanoparticles with APTES (MNP-NH_2)

250 mg of prepared magnetite was dispersed in 100 mL of ethanol and sonicated for 15 min. The resulting dispersion was diluted with 300 mL of ethanol and then sonicated for further 30 min. 1.8 eq of APTES solution (8.62 g) was added to the dispersion under nitrogen atmosphere and the reaction mixture was stirred vigorously at room temperature for 16 h.

The resulting amino functionalized (Fe_3O_4-NH_2) nanoparticles were magnetically recovered and washed with ethanol and DCM several times and then dried under vacuum

2.4. Preparation of alkyne functionalized MNP (MNP-Alky)

300 mg of MNP-NH_2 was dispersed in 10 mL of dichloromethane using an ultrasonic bath for 10 min. (223 mg, 31.8 mmol) of propargyl acid, (220 mg, 31.8 mmol) of DCC and (13 mg, 3.18 mmol) of DMAP were then added and the mixture was magnetically stirred for 16 h under nitrogen atmosphere at room temperature. The solid product was recovered with magnetic field and washed with ethanol (8 × 10 mL), then with a mixture of H_2O/t-BuOH(1/1) (4 × 4 mL) and finally with dichloromethane (several times) to ensure the removal of the urea by-product formed during the reaction. The resulting product was dried under vacuum and stored in a desiccator.

2.5. Preparation of triazole functionalized MNP (MNP-Trz)

The catalytic 1,3-dipolar cycloaddition of alkyne functionalized magnetite with 4-Azido-1-nitrobenzene was carried out under the following conditions (Zhou et al., 2008). 800 mg of alkyne functionalized magnetite and (355 mg, 2.1621 mmol) of 4-azido-1-nitrobenzene were mixed with 6.5 mL of tBuOH/H_2O (1:1). 650 μL of freshly prepared 1 M aqueous solution of sodium ascorbate (0.65 mmol) and 217 μL of 1 M aqueous solution of copper sulfate pentahydrate (0.065 mmol) were added. The mixture was stirred at room temperature for 48 h. The final product was recovered by an external magnet and washed several times with ethanol and subsequently with deionized water and then dried.

2.6. Preparation of silica coated MNP (Fe_3O_4@SiO_2)

To protect MNP from oxidation reaction and improve their dispersion in water, they were coated with a silica layer using the alkaline hydrolysis of TEOS. In a 250 mL round-bottom flask, 100 mg of magnetite (Fe_3O_4), dispersed in a mixture of 80 mL of anhydrous ethanol and 20 mL of deionized water, was sonicated for 15 min. The pH was adjusted to pH = 9 with ammonia solution (28%) and then 200 μL of TEOS was added. The reaction was stirred for 4 h at room temperature under nitrogen atmosphere. Finally, the product was recovered with an external magnet and washed several times with deionized water and then with ethanol.

2.7. Preparation of functionalized silica coated MNP (MNPS-NH_2, MNPS-Alky, MNPS-Trz)

These materials were prepared by the same procedure used of Fe_3O_4 particles using as starting compound Fe_3O_4@SiO_2.

2.8. Characterization

The specific surface areas of the modified and functionalized Fe_3O_4 nanoparticles were performed by N_2-adsorption and desorption at −196 °C, using Micromeritics Gemini VII instrument. Before measurement, each sample was degassed at 200 °C for 24 h under N_2 flow. Surface areas were calculated using Brunauer-Emmett-Teller (BET) equation.

Infrared spectroscopies were carried out with a Jasco-4200 Fourier transform infrared spectrometer (Jasco Inc., Easton, MD, USA) using KBr pellets in the 4000–400 cm^{-1} region. The dry powders of magnetic particles were blended with KBr, ground and pressed into disks for measurements.

Powder X-ray diffraction (XRD) patterns of magnetic nanoparticles were collected with a Bruker-D8 advance AXS diffractometer with CuKα radiation λ = 1.5418A° operating at 40 kV, 40 mA. The scanning rate was 2°/min and the scanning scope of θ was from 2° to 20 at room temperature.

Thermogravimetric analysis of particles was performed with a TG 209 Netzsch apparatus. Alumina crucibles were filled with accurately weighted samples of about 10 mg. The temperature program ranged from 35 °C to 813 °C at a heating rate of 10 °C/min. All experiments were conducted under nitrogen atmosphere. The weight loss was recorded as a function of temperature and time.

Size measurements of aqueous solutions of magnetic nanoparticles were done by Zetasizer nanoseries "zs" of Malvern instruments (England). DTS nano program was used for data evaluation. The following Stokes–Einstein law was used to compute the mean droplet diameter: $D_H = K_B T/(3\pi\eta D)$, where D_H, K_B, T, η and D are the hydrodynamic diameter of the particles, Boltzmann constant, temperature in Kelvin, viscosity of the medium and diffusion coefficient, respectively. Zeta potentials of magnetic nanoparticles were determined as function of pH values using the Malvern Zetasizer via electrophoretic mobility measurements. Different pH solutions were prepared using 1 mM NaCl solution and the pH values were adjusted by 1 mM NaOH or 1 mM HCl solution using a pH meter. The samples were diluted in the corresponding solution before measuring the electrophoretic mobility.

Transmission Electron Microscopy, TEM, was performed with a Philips CM120 microscope at the "Centre Technologique des Microstructures" (CTμ) at the University of Lyon (Villeurbanne, France). Before observation, carbon grids were plunged in nanoparticles powder, and the excess was then removed. The samples were observed by TEM under 120 kV acceleration voltages.

Scanning Electron Microscopy, SEM, was performed with a FEI Quanta 250 FEG microscope at the "Centre Technologique des Microstructures" (CTμ) at the University of Lyon (Villeurbanne, France). Powder was deposited on a flat steel holder. The sample was coated under vacuum by cathodic

sputtering with copper (10 nm). The samples were observed by SEM under an accelerating voltage of 15 kV.

The magnetization properties of the samples were examined by an automatic bench for magnetic measurement (ABMM) at CNRS-IRC laboratory Lyon. Magnetization of the samples was investigated by decreasing magnetic field (H) from 20,000 to 15,000 Oersted.

2.9. Adsorption and desorption experiments

The adsorption of various metal cations Cu^{2+}, Zn^{2+} and Pb^{2+} on magnetic dispersions (functionalized magnetic nanoparticles MNP-Trz and silica coated homologous MNPS) was carried out on the basis of batch equilibrium technique in aqueous medium at 25 °C. In a typical experiment, 2 mg of MNP-Trz or MNPS-Trz is mixed with 2 mL of appropriate aqueous solution containing (50–600 ppm) of metal ions for 4 h at 250 rpm to reach the adsorption equilibrium. The amount of residual cation in the solution was measured with flame atomic absorption spectrometer (Perkin Elmer 700) after magnetic separation of chelated MNP from the supernatant.

The adsorption capacity q_e (mg g^{-1}) of metal ions in the presence of magnetic dispersion at equilibrium state was calculated according to Eq. (2):

$$q_e = \frac{(C_0 - C_e)V}{M} \quad (2)$$

where C_0 (mg L^{-1}) is the initial concentration of metal ion, C_e (mg L^{-1}) is the equilibrium concentration in solution, V (L) is the total volume of solution, and M (g) is the sorbent mass.

For kinetic studies, the initial concentration of metal ion (Cu^{2+}, Zn^{2+} and Pb^{2+}) was 400 mg.L^{-1} and the initial pH value was 5.5. The contact time was varied under a stirring rate of 250 rpm at 25 °C. The effect of pH solution on metal ion adsorption at equilibrium state was studied for each initial metal ion concentrations of 400 mg L^{-1}. The pH values varied from 2 to 6 by adjusting the initial metal ion solution with NaOH or HCl. The adsorption studies were carried out at 250 rpm for 4 h at room temperature. Duplicate experiments were carried out for each experiments and the high reproducibility was obtained.

The desorption efficiency studies were conducted with dilute HNO_3 solution concentration range of 0.1–0.2 mol L^{-1} as desorption medium. Adsorption was firstly conducted using 20 mg of MNP-Trz in 400 mg L^{-1} Pb^{2+} solution for 4 h at room temperature. The resulting Pb^{2+} sorbed MNP-Trz containing 136 mg g^{-1} of lead ions was used to carry out the desorption study. 10 mL of HNO_3 solution was added to 10 mg of this material and then stirred at 250 rpm during variable time ranging from 5 min to 250 min at 25 °C. The MNP-Trz particles were collected by an external magnetic field and the concentration of Pb^{2+} ions was determined via supernatant analysis.

The desorption efficiency studies were conducted with dilute HNO_3 solution concentration range of 0.1–0.2 mol L^{-1} as desorption medium. Adsorption was firstly conducted using 20 mg of MNP-Trz in 400 mg L^{-1} Pb^{2+} solution for 4 h at room temperature. The resulting Pb^{2+} sorbed MNP-Trz containing 136 mg g^{-1} of lead ions was used to carry out the desorption study. 10 mL of HNO_3 solution was added to 10 mg of this material and then stirred at 250 rpm during variable time ranging from 5 min to 250 min at 25 °C. The MNP-Trz particles were collected by an external magnetic field and the concentration of Pb^{2+} ions was determined via supernatant analysis.

The desorption efficiency DE (%) was determined using the following Eq (3):

$$DE = C \times V/q \times M \times 100\% \quad (3)$$

where C (mg L^{-1}) is the concentration of copper ions in the desorption solution, V (L) is the volume of the desorption solution, q (mg g^{-1}) is the amount of copper ions adsorbed on the adsorbent before desorption experiment, and M (g) is the mass of the adsorbent used in the desorption experiments. The consecutive process of adsorption-desorption was performed three times.

3. Results and discussion

3.1. Synthesis and characterization of functionalized MNP

The synthetic pathway used to prepare MNP functionalized with 1,2,3-triazole units is shown in Scheme 1. Firstly, magnetite nanoparticles NPs (Fe_3O_4) were synthesized by coprecipitation method from Fe^{2+} and Fe^{3+} solutions. The XRD spectrum (Fig. 1) confirms the cubic spinel structure of magnetite with six characteristic peaks 2θ = 30.3°, 35.6°, 43.1°, 53.7°, 57° and 62.7° which may be indexed as (220), (311), (400), (422), (511) and (440) respectively. These data matched well with those of literature data (Wang et al., 2010). The lattice constant was found to be 8.37 $\dot{A}$ which is of the same order of magnitude as the lattice parameter of magnetite (8.39 $\dot{A}$) (Mahdavian and Mirrahimi, 2010).

Three step synthetic strategy was used to surface modification of Fe_3O_4 NPs. Magnetite particles reacted with 3-aminopropyltriethoxysilane (APTES) and were then subsequently added to propargyl acid to introduce alkyne functions using Steglich esterification in the presence of DCC and DMAP. The 1,3-dipolar cycloaddition of the latter compound with 4-nitroarylazide derivative in click chemistry conditions affords the triazole-based NPs (MNP-Trz).

Silica coated magnetite NPs have been also prepared in this work. Such encapsulation should ensure better stability of Fe_3O_4 core toward chemical attacks especially oxidation reactions and favors dispersion of nanoparticles in aqueous solution. The silica shell was introduced by the alkaline hydrolysis of TEOS with ammonia solution followed by functionalization using the same procedure used for Fe_3O_4 NPs.

FTIR analysis was used to confirm the surface modification of MNP for the different synthesis steps (Fig. 2). Magnetite spectrum reveals an intense peak at 569 cm^{-1} related to Fe—O vibrations. The occurrence of the characteristic peaks of primary amine group at 3427 cm^{-1} and 1631 cm^{-1}, of C—H stretching vibrations at 2921 cm^{-1} and 2852 cm^{-1} and of Si—O stretching at 1027 cm^{-1} indicates that the APTES has been successfully coupled to the surface of magnetite particles. The spectrum of MNP-Alky shows the appearance of peaks related to the newly formed alkyne and amide functions at 2121 cm^{-1} (≡C—H stretching) and 1650 cm^{-1} (C═O stretching). After the click reaction, the vibration band related to ≡C—H group at 2121 cm^{-1} disappeared and several new bands appear between 1374 and 1670 cm^{-1} indicating the pres-

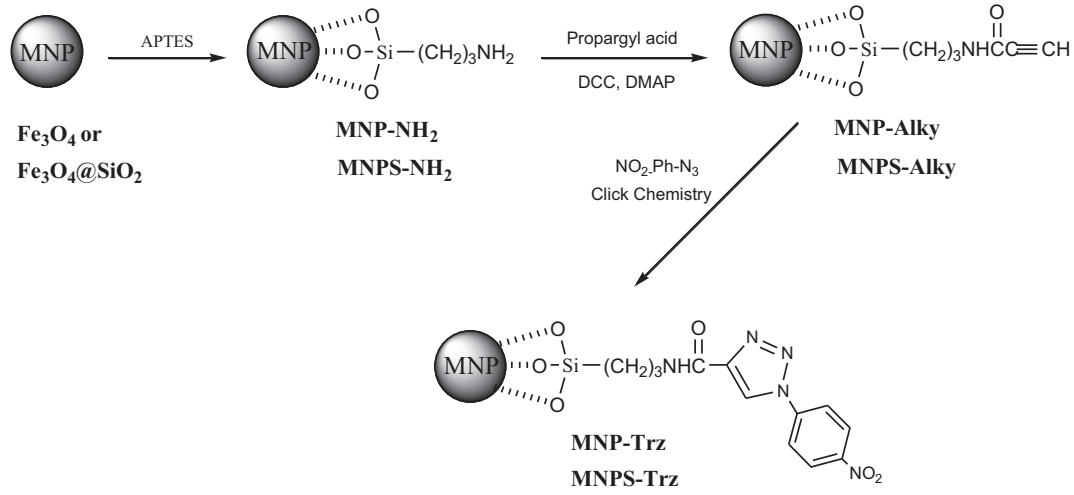

Scheme 1 A schematic representation for preparation of modified silica coated and uncoated magnetite-triazole nanoparticles.

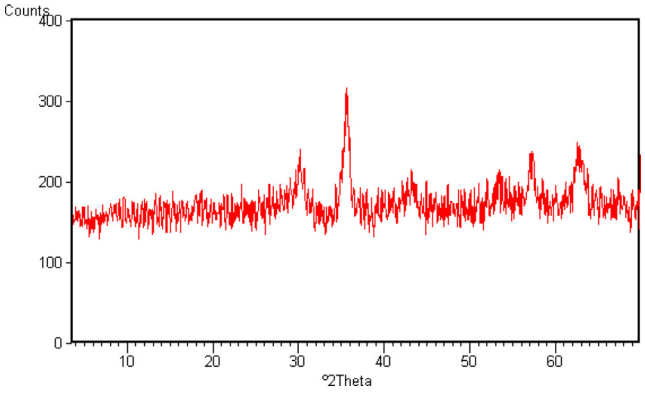

Figure 1 Powder X-ray diffraction (XRD) of magnetite Fe_3O_4.

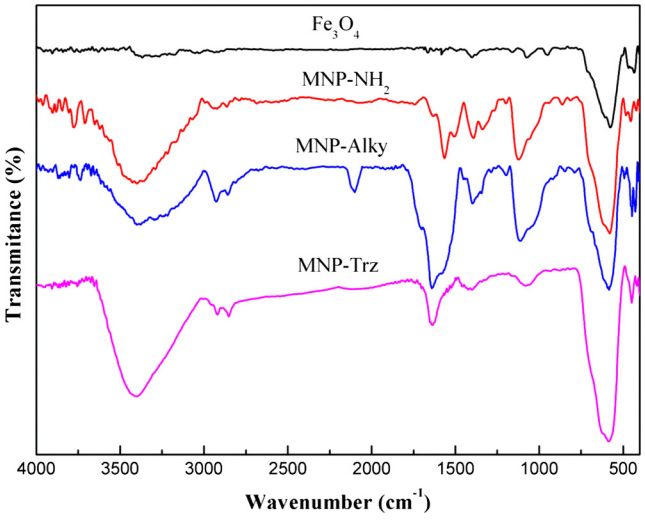

Figure 2 FTIR spectra of (a) Fe_3O_4, (b) MNP-NH_2, (c) MNP-Alky, (d) MNP- Trz magnetic nanoparticles.

ence of 1,2,3-triazole heterocycle in particular at 1393 cm^{-1}, 1563 cm^{-1} and 1529 cm^{-1} related to C—N, C═C and N═N vibrations. Similar IR characteristics were obtained for MNPS series (Fig. S1, supplementary file). The silica-modification was confirmed in Fe_3O_4@SiO_2 spectrum by the presence of 3 bands at 1056, 794 and 973 cm^{-1} corresponding to the stretching vibrations of Si—O—Si, Si—OH and Si—O—Fe respectively.

Thermogravimetric analysis was used to estimate the degree of modification for intermediate and final magnetic materials. The relative comparison between weight losses of each sample with the previous one indicates the progress of modification (Fig. 3). The weight loss of Fe_3O_4 MNP in the investigated thermal range was found to be around 4.39% and involves the evaporation of physically and chemically adsorbed water. It occurs on 3 steps: A first weigh loss of 2.15% was observed below 125.5 °C related to the evaporation of adsorbed water followed by a weight gain between 125.5 °C and 151 °C which was also previously reported by Caruntu et al. (2004) and Cao et al. (2009) and was attributed to the oxidation of magnetite Fe_3O_4 to maghemite Fe_2O_3. The final step corresponds to dehydration of OH groups.

The weight losses relative to the crude MNP for MNP-NH_2, MNP-Alky and MNP-Trz are 1.54 wt.%, 6.83 wt.%

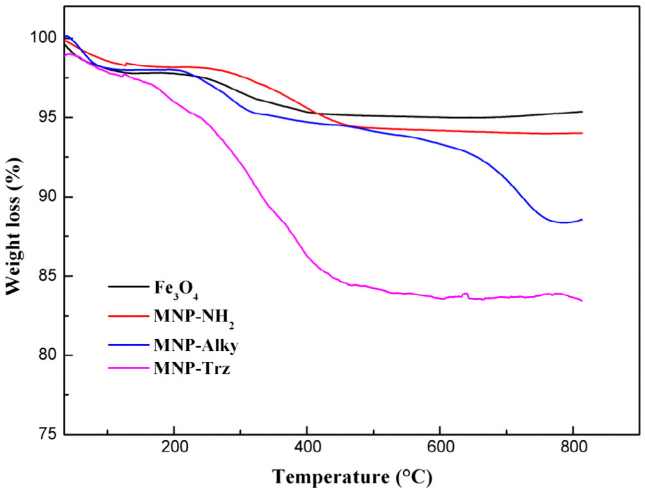

Figure 3 TGA thermograms of (a) Fe_3O_4, (b) MNP-NH_2, (c) MNP-Alky, (d) MNP- Trz magnetic nanoparticles.

and 11.94 wt.%, respectively. The quantity of APTES immobilized onto the surface of MNP, determined from the weight loss under the assumption that all the ethoxy group were eliminated during grafting of APTES to Fe_3O_4 core and that only the organic part of the linker contributes to the mass loss was estimated and found to be 0.28 mmol/g of magnetite.

TGA data of Fe_3O_4@SiO_2 show that the quantity of silica shell grafted on Fe_3O_4 core was around 1.89 wt.%. MNPS-NH_2, MNPS-Alcy and MNPS-Trz exhibit the same thermal degradation profiles with weight losses of 6.01 wt.%, 7.60 wt.% and 10.53 wt.% respectively corresponding to the organic functional group decomposition (Fig. S2. supplementary file).

The morphology and the size of neat Fe_3O_4 and Fe_3O_4@-SiO_2 NPs and their functionalized analogues were studied by TEM. Some typical TEM images are shown in Fig. 4a–c. All investigated particles have a spherical shape with a low particle size polydispersity. The mean particle size is almost the same for crude and functionalized magnetic particles, which is around 9.6 nm. This indicates that the used chemical reactions occur only at the surface of magnetic particles and have no drastic effect on the colloidal stability of the dispersion.

Similar results, i.e. size and spherical shape of investigated MNP were obtained by SEM analyses (Fig. 4e–f). Particle sizes obtained by dynamic light scattering were however much larger than those deduced from TEM and SEM images. This can be explained by the possible low aggregation of particles after various magnetic separation and redispersion cycles.

The effect of pH on zeta potential (ζ) of MNP was also investigated and confirmed the immobilization of triazole units. As shown in Fig. 5, the magnetite particles are positively charged at lower pH and negatively charges at higher pH. The isoelectric point (IEP) was found to be around pH of about 6.45 consistent with the values reported in the literature (Badruddoza et al., 2011; Takafuji et al., 2004). After modification of the particles with APTES, the IEP shifted to 8.2 close to the pKa of primary amine group) revealing the presence of amine groups on MNP-NH_2 particles. The positive zeta potential below the IEP is attributed to the protonation of amine groups on the particle surface (Xu et al., 1997).

Since tertiary amines gave rise to less protonation reactions then primary amines of APTES, the IEP of MNP-Trz shifted from 10 to 4.3 after cycloaddition reaction leading to the formation of triazole synthons and revealed that the amino-functionalized magnetic nanoparticles were positively charged at pH < 4.3 and negatively charged at pH > 4.3. These results confirmed the triazole functionalization of MNP.

Similar results were obtained for silica-coated magnetite (plot is shown in Supplementary file Fig. S3). The IEP of silica-coated magnetite nanoparticles Fe_3O_4@SiO_2 was at pH = 3, and is in good agreement with reported values (Karatapanis et al., 2011).

The magnetic properties of Fe_3O_4, MNP-NH_2, MNP-Trz and their silica coated homologous were investigated by vibrating sample magnetometer (VSM). Typical hysteresis curves are depicted in Fig. 6. All samples exhibit superparamagnetic behavior without remanence or coercivity. This feature indicates that these particles are responsive to an external magnetic field without residual magnetism after removal of the applied magnetic field. The saturation magnetization values (Ms) for Fe_3O_4, MNP-NH_2, and MNP-Trz nanoparticles are 59.07, 58.68 and 43.10 emu/g respectively. The relatively slighter Ms value of Fe_3O_4 MNP in comparison with bulk magnetite (92 emu/g) was already reported in previous study and explained by the rather small size of the Fe_3O_4 MNP prepared by co-precipitation method (Feng et al., 2008). The triazole-functionalized MNP shows lower magnetization value than crude magnetite particles probably due to the presence of non-magnetic materials on the surface of nanoparticles such as passivation non-magnetic layer.

No specific effect on superparamagnetic properties was observed for silica coated nanoparticles in comparison with Fe_3O_4 NPs ($Ms_{(MNP\text{-}Trz)}$ = 43.1 emu/g, $Ms_{(MNPS\text{-}Trz)}$ = 47.66 emu/g) supporting the idea that both particle series could be detected easily and can be used for separation of metal-adsorbed MNP. The lower plateau values obtained for silica series except for MNPS-Trz are due to the magnetic silica shell surrounding the magnetite core. For this latter material, the slightly lower functionalization percentage detected by TGA analysis (10.53 wt.% for MNPS-Trz and 11.94 wt.% for MNP-Trz) should be at the origin of the slightly higher magnetization value.

The surface area calculated by BET analysis of neat magnetite Fe_3O_4, Fe_3O_4@SiO_2 and the triazole-functionalized NPs MNP-Trz was determined by nitrogen sorption measurements and was found to be 90.65, 94.96 and 119.35 $m^2\ g^{-1}$ respectively (Figs. S4–S5, Supplementary file). The surface areas of crude and silica-coated Fe_3O_4 are substantially similar suggesting similar morphological properties of these materials.

3.2. Triazole-based magnetic nanoparticles for heavy metal adsorption

3.2.1. Effect of initial pH

The pH of the aqueous solution is a critical controlling parameter in the adsorption process. Thus, it is important to determine the optimum pH value for better metal ion adsorption on synthesized magnetic nanoadsorbents.

The effect of pH on the adsorption of Cu^{2+}, Zn^{2+} and Pb^{2+} ions by synthesized MNP-Trz nanoparticles was investigated at 25 °C and at initial ion concentration of 400 mg L^{-1}. The investigated pH range was 1–6 since at higher pH values copper, zinc and lead ions precipitated as $Cu(OH)_2$, $Zn(OH)_2$ and $Pb(OH)_2$, respectively.

The evolution of adsorption ability of magnetic particles as a function of pH v is illustrated in Fig. 7. It can be seen that the adsorption ability is strongly pH dependent and increased along with increasing pH value in the range of 2–5 but changed slightly above pH 5.

To explain this feature, two aspects should be considered. First, the surface composition of metal oxide adsorbent may undergo protonation/deprotonation reaction depending on pH solution as expressed in Scheme 2, and secondly the ion species present at investigated pH media.

Thereby, in high acidic solution, the occurrence of high proton concentrations induces competitive adsorption reactions of proton ions for existing adsorption sites resulting in lower metal ion adsorption. Furthermore, the positively charged surface of MNP as illustrated in schema 2 induces electrostatic repulsions of Cu^{2+}, Zn^{2+} and Pb^{2+} ions' disadvantaging adsorption process.

Another reaction that may take place at the surface of triazole functionalized MNP surface in strong acid media is related to the protonation of the triazole heterocycles to pro-

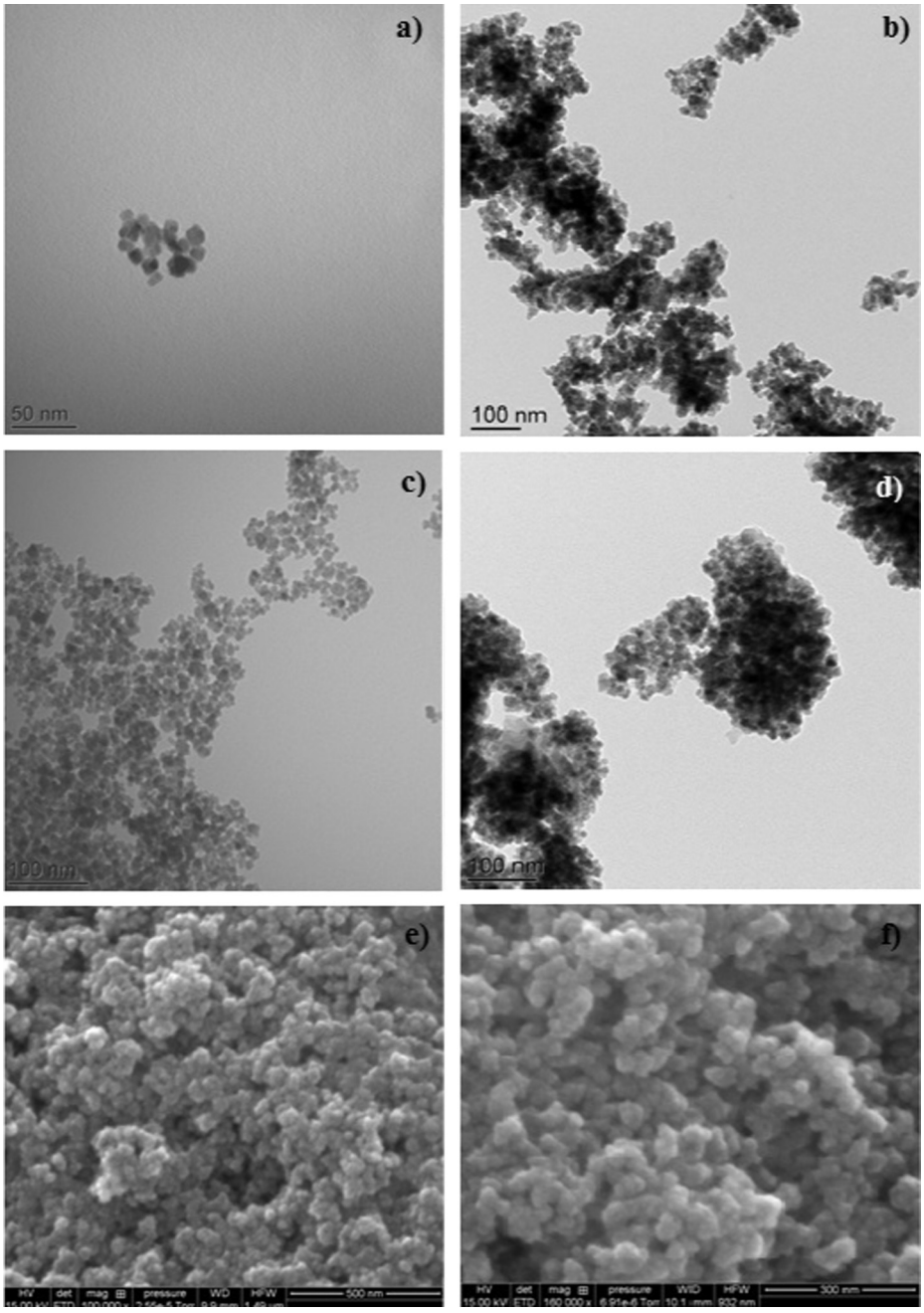

Figure 4 TEM images of (a) neat Fe_3O_4, (b) Fe_3O_4@SiO_2, (c) MNP-NH_2, (d) MNP- Trz; SEM images of (e) neat Fe_3O_4, (f) MNP-Trz magnetic nanoparticles.

duce a protonated 1,2,3-triazolium salts (Scheme 2) which can also be involved in electrostatic repulsive interactions responsible of low affinity between magnetic nanoparticles and metal ions in acidic (Yacob and Liebscher, 2015).

As pH values increased, the involved repulsive electrostatic interactions become weaker and the negatively charged MNP, as demonstrated by zeta potential values for $pH > pH_{IEP} = 4.3$, attracts the positively charged metal ions. In this condition, the nitrogen atoms of 1,2,3-triazole moiety may act as N donor ligands and the unpaired electron of nitrogen atoms could create coordination bonds with M^{2+} ions leading to mono, di or trinucleating ligand architectures (Badruddoza et al., 2011). Meantime, the competition of proton adsorption sites becomes less significant. Both effects result in enhancement of sorption capacity.

As shown in Fig. 7, it is interesting to notice that the adsorption capacity for Pb^{2+} ions is higher than that for Cu^{2+} and Zn^{2+} irrespective of pH, suggesting the possible selectivity of magnetic nanoadsorbents for Pb^{2+}.

3.2.2. Adsorption isotherm

Adsorption isotherm describes how adsorbate (pollutant) interacts with adsorbent. To understand the adsorption mechanism for a better effective use of the nanoadsorbent, it is important to correlate the experimental equilibrium data with

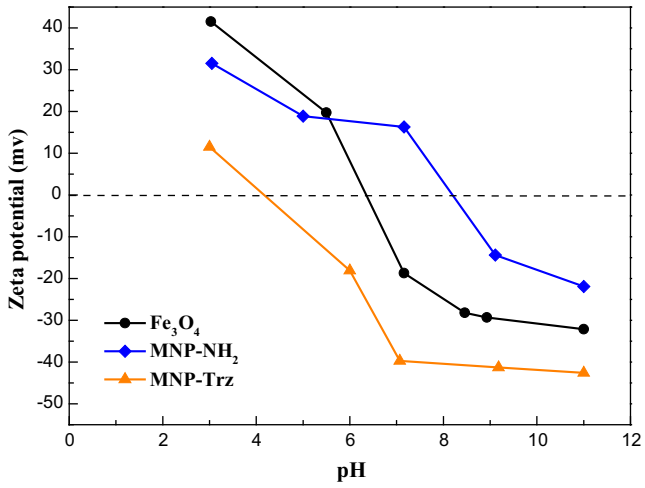

Figure 5 Zeta potential of crude Fe_3O_4, MNP-$NH_2$and MNP-Trz magnetic nanoparticles as function of pH in 1 mM NaCl solution.

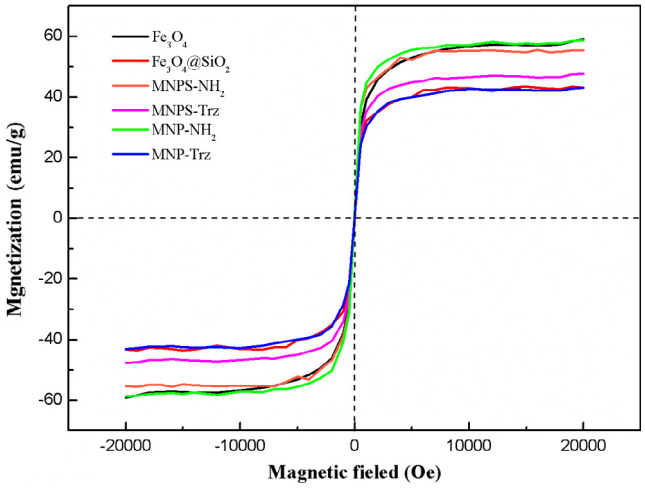

Figure 6 Magnetization curves of MNP and MNPS nanoparticles at room temperature.

the theoretical or empirical models. In the present work, the equilibrium data were analyzed according to Langmuir and Freundlich models expressed by Eqs. (4) and (5), respectively.

$$\frac{C_e}{q_e} = \frac{C_e}{q_m} + \frac{1}{K_L q_m} \tag{4}$$

$$lnq_e = lnK_F + \frac{1}{n} lnC_e \tag{5}$$

where q_e (mg g^{-1}) represents the amount of metal ions adsorbed on the absorbent at equilibrium; C_e (mg L^{-1}), the equilibrium ion concentration in solution; q_m (mg g^{-1}), the maximum adsorption capacity of the adsorbent corresponding to complete monolayer coverage; K_L (L mg^{-1}), the Langmuir adsorption equilibrium constant; K_F (L mg^{-1}), the Freundlich constant and n is the heterogeneity factor that lies for favorable adsorption process in the range of 1–10.

The Langmuir model assumes that adsorption takes place at specific homogeneous sites within the adsorbent and is usually applied for many monolayer adsorption processes while the Freundlich model describes heterogeneous adoption systems.

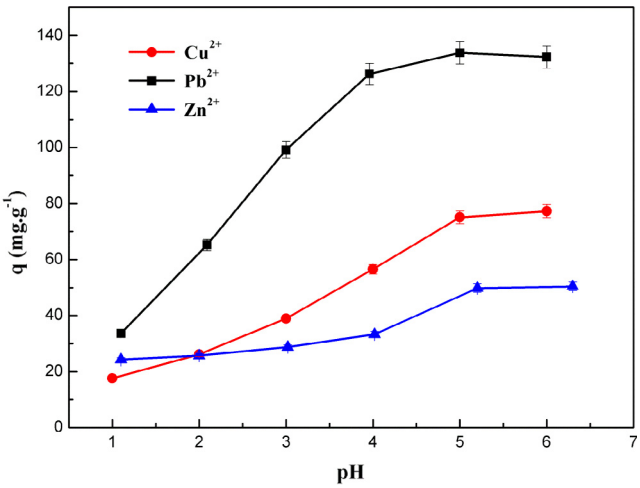

Figure 7 Effect of pH on the adsorption capacity of Cu (II), Pb (II) and Zn(II) metal ions by MNP-Trz in aqueous solution. Initial concentration of metal ions 400 mg L^{-1}; reaction time 240 min; mixed 250 rpm at T = 25 °C.

The equilibrium isotherms for the adsorption of Cu^{2+}, Zn^{2+} and Pb^{2+} ions by MNP-Trz at pH 5.5 and 25 °C are shown in Fig. 8. Initial metal ion concentrations varied from 50 to 600 mg L^{-1}. It can be seen that the equilibrium adsorption capacity (q_e) of the metal ions increased with increasing the equilibrium ion concentrations in aqueous solution (C_e) until reaching equilibrium.

The Langmuir and Freundlich parameters are determined and summarized in Table 1 and Fig. 9. The values of q_m and K_L were determined from the slope and intercept of the linear form of Langmuir equation C_e/q_e versus C_e and K_F and $1/n$ parameters from the intercept and slope of the linear form of the Freundlich equation ln q_e versus ln C_e. It can be seen from the best fitting parameter R^2 values, that Langmuir model fits the experimental data better than Freundlich model suggesting a monolayer homogeneous adsorption.

The dimensionless constant separation factor R_L, which is considered as the more reliable indicator for the adsorption capacity, was evaluated according to the following equation:

$$R_L = \frac{1}{1 + K_L C_0} \tag{6}$$

where K_L (L g^{-1}) is the Langmuir constant and C_0 is the initial concentration (mg L^{-1}). The calculated R_L values are gathered in table 1 and are between 0 and 1 indicating that the adsorptions of metal ions are favorable.

The maximum adsorption values obtained by Langmuir isotherm were 87.87, 167.78 and 51.20 mg g^{-1} for Cu^{2+}, Pb^{2+} and Zn^{2+}, respectively and are in accordance with the obtained experimental values. We can deduce the following capacity order: $Pb^{2+} > Cu^{2+} > Zn^{2+}$.

This selectivity series could be the result of various factors related to the electronic properties of different atoms present in the ligand as well as metal ion properties which govern the complexation process. It is known that the higher the metal ionic potential (which is related to metal ion charge/radius

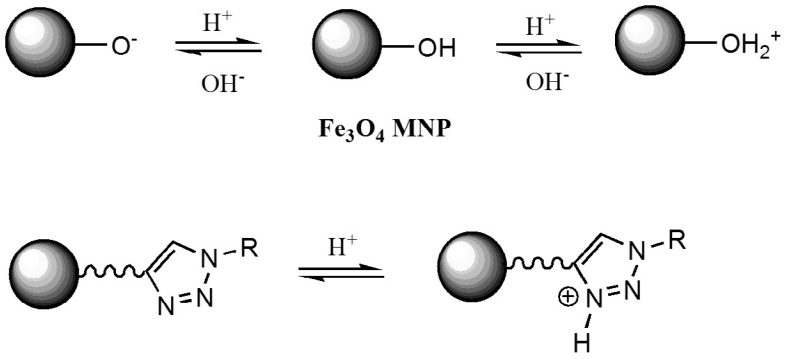

Scheme 2 Protonation/deprotonation reactions of MNP in aqueous solution.

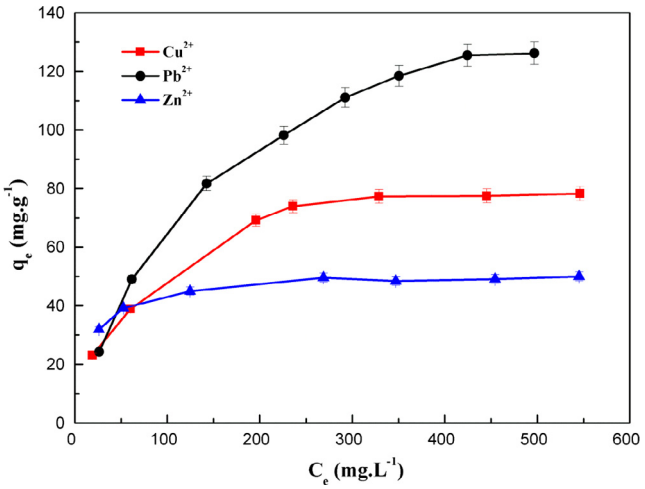

Figure 8 Equilibrium isotherms of Cu(II), Pb(II) and Zn(II) metal ions by MNP-Trz in aqueous solution. Initial pH = 5.5; reaction time 240 min; mixed 250 rpm at T = 25 °C.

ratio), the higher will be its tendency to attract electrons of the ligand, and hence the complex formed will be the most stable (Gurdeep, 2010). For cations having the same charge, the stability of complexes decreased with increasing of the ionic radii; smaller is the ion, easier it reacts with the ligand. The hydrated ion sizes of the metal increased in the order Pb^{2+} (4.01 A°) < Cu^{2+} (4.19 A°) < Zn^{2+} (4.30 A°) (Calvo et al., 2009). This classification is consistent with the obtained capacity order.

Zhu and al. reported the application of xanthate-modified magnetic chitosan for the removal of multi-metal Pb(II), Cu (II) and Zn(II) solutions. Based on the covalent index of metal ion $X_m^2 r$ where X_m is electronegativity and r is ionic radius, they obtained the same order of preference of metal ions onto magnetic chitosan particles. The higher covalent index of Pb(II) ions indicated its stronger attraction to the lone pair of electrons in sulfur and nitrogen atoms of xanthate-modified chitosan to form complexes (Zhu et al., 2012).

The maximum uptakes of Cu^{2+}, Zn^{2+} and Pb^{2+} by MNP-Trz particles obtained on this work are compared with results reported in literature for other magnetic adsorbents as shown in Table S1 - Supplementary file. In general, the MNP-Trz particles prepared and used in this work have higher adsorption capacities and then reported adsorbents, except for (Acrylic acid-crotonic acid) copolymer-modified magnetic nanoparticles (Ge et al., 2012). For this latter material, the content of polymer was estimated to 36.7% in weight bases on the total weight of modified MNP. The lower density of triazole synthons in our material (11.94 wt.%) should be at the origin of the lower adsorption capacity.

3.2.3. Adsorption kinetics

The adsorption kinetic of metal ions was investigated for initial metal ion concentration of 400 mg L^{-1} at pH = 5.5 and at 25 °C. The obtained results are illustrated in Fig. 10.

The equilibrium was reached for copper and Zinc ions at ~ 175 min and at ~ 240 min for lead ion. These results are in good agreement with data reported for adsorption of different metal ions onto Fe_3O_4 based nanoadsorbents for which similar equilibrium times were described (Zhu et al., 2012).

The uptake–time curves show that the maximum uptake follows the order Pb^{2+} > Cu^{2+} > Zn^{2+}.

A stirring time of 4 h was used in all further adsorption experiments to ensure equilibrium.

Table 1 Parameter values of Langmuir and Freundlich isotherms for adsorption capacity of Cu (II), Pb (II) and Zn(II) metal ions onto MNP-Trz at 25 °C.

Metal ions	Langmuir				Freundlich		
	q_m (mg g^{-1})	K_L (L g^{-1})	R_L range	R^2	n	K_f (L g^{-1})	R^2
Cu^{2+}	87.87	0.0176	0.0835–0.5738	0.9965	2.59	7.97	0.9523
Pb^{2+}	167.78	0.0065	0.1966–0.7508	0.9982	1.79	4.45	0.9708
Zn^{2+}	51.20	0.0632	0.0258–0.2137	0.9996	7.21	21.72	0.9099

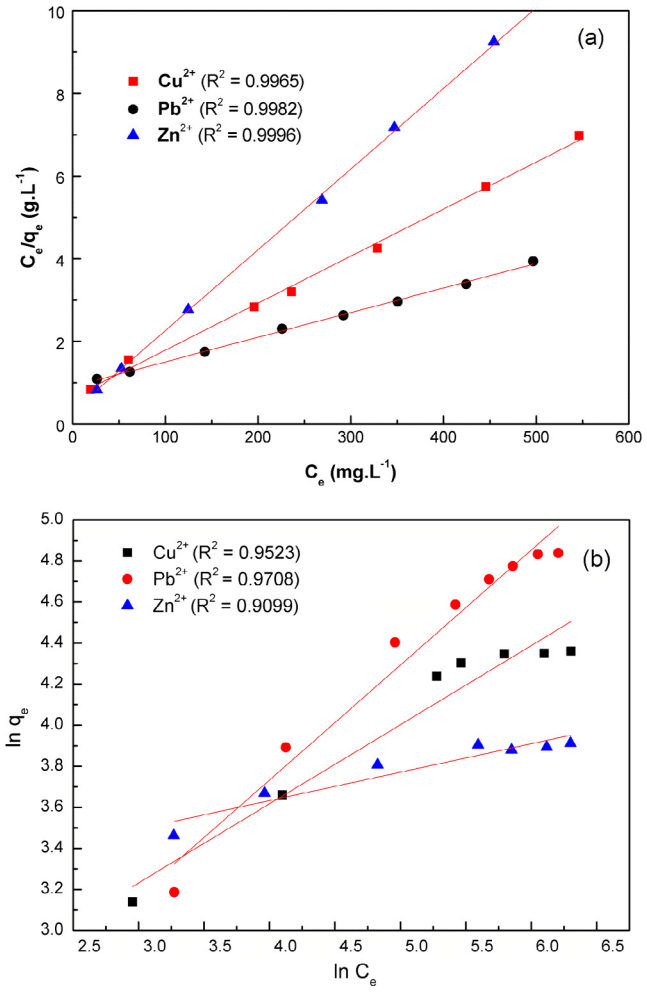

Figure 9 The Langmuir (a) and Freundlich (b) isotherm plots of Cu(II), Pb(II) and Zn(II) metal ions by MNP-Trz

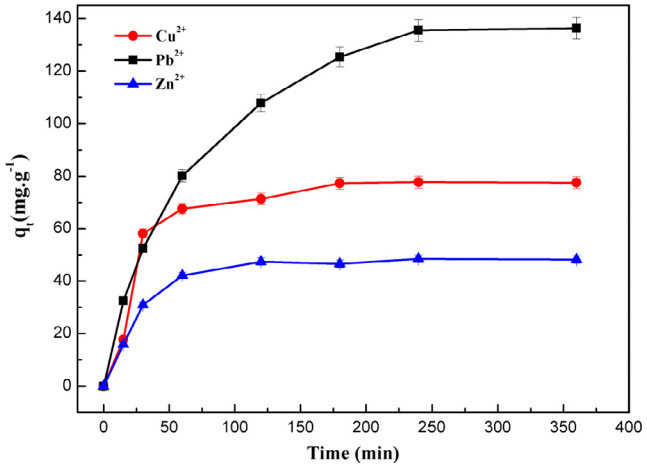

Figure 10 Effect of contact time on adsorption capacity of Cu (II), Pb (II) and Zn(II) metal ions onto MNP-Trz at 25 °C.

In order to examine the controlling mechanism of adsorption, several kinetic models are used to fit experimental data. We used in this work the pseudo first-order and second-order models expressed by the following equations:

Pseudo-first order kinetic:

$$ln(q_e - q_t) = lnq_e - k_1 t \quad (7)$$

Second order kinetic:

$$\frac{t}{q_t} = \frac{1}{k_2 q_e^2} + \frac{1}{q_e} t \quad (8)$$

where q_t (mg g^{-1}) is the adsorption at time t (min); q_e (mg g^{-1}) is the adsorption capacity at equilibrium, and k_1 (min^{-1}) and k_2 (g mg^{-1} min^{-1}) are the kinetic rate constants for the pseudo-first order and second order models respectively.

The kinetic parameters obtained from these models are tabulated in Table 2 and the plots for both models are given in Fig. 11. It is found that for all investigated metal ions, the correlation coefficients (R^2) for the second order kinetic are higher than those of pseudo-first order. Furthermore, the adsorption capacity values at equilibrium q_e obtained from the slope of the plot of the second order equation (t/q_t against t) are more consistent with the experimental q_e values than those obtained from the slope of the pseudo-first order plot. It is clear that the adsorption kinetic of metal ions on magnetic nanoparticles material followed this model, revealing that chemisorption might be the rate-limiting step that controls the adsorption process. Usually, for magnetic nanoparticles bearing surface chelating functional groups, the main mechanism controlling the adsorption process is a chelating exchange process following a second-order chemical reaction (Fu and Wang, 2011).

3.2.4. Comparison of adsorption behavior of MNP-Trz and MNPS-Trz

The effect of silica shell on adsorption behavior of triazole functionalized particles was investigated for Pb^{2+} ions in standard conditions (pH = 5.5, T = 25 °C, 250 rpm). We noticed the same kinetic profile (Fig. 12) with a slightly higher metal uptake for MNPS-Trz material (q_e (MNP-Trz) = 136.3 mg g^{-1}, q_e (MNPS-Trz) = 145.1 mg g^{-1}). This feature should be the result of involvement of silanol group on complexation behavior according to the following equation (Hu et al., 2010).

$$Si{-}OH + Pb^{2+} + H_2O \Longleftrightarrow Si{-}O^{-}(PbOH)^{+} + 2H^{+} \quad (9)$$

The silica coated particles could be used as an efficient adsorbent with reliable chemical stability and good dispersion in aqueous media.

3.2.5. Desorption study

Desorption study was conducted for Pb^{2+} pre-adsorbed on MNP-Trz to explore the possibility of recyclability of the magnetic nano-adsorbent. Referring to the pH effect on adsorption efficiency of MNP-Trz, it was expected that acid media with pH below 2 would be effective for desorption. Ge et al. reported that the desorption ratio of metal ions increased as H^+ concentration increased and reached an optimal value for ~0.1 mol L^{-1} beyond which the magnetic adsorbent was corroded by acid media (the adsorbent is completely destroyed at 2 mol L^{-1} after 3 h) (Ge et al., 2012).

Thus, Pb^{2+} preadsorbed on MNP-Trz dealt with weakly acidic HNO_3 solution in concentration range of 0.1–0.2 mol L^{-1}. As shown in Fig. 13, desorption ratio of adsorbed ions increased as a function of time and HNO_3 concentration. A constant desorption efficiencies of 88% were reached for

Table 2 Kinetic parameters for Cu^{2+}, Pb^{2+} and Zn^{2+} ion adsorption by MNP-Trz.

Metal ions	$q_{e\ (exp)}$ (mg g^{-1})	Pseudo-first order			Second order		
		k_1 (min^{-1})	q_e (mg g^{-1})	R^2	k_2 (g mg^{-1} min^{-1})	q_e (mg g^{-1})	R^2
Cu^{2+}	77.3	0.01581	31.07	0.8681	6.93 10^{-4}	82.37	0.9973
Pb^{2+}	136.3	0.01376	128.68	0.9166	1.04 10^{-4}	162.34	0.9970
Zn^{2+}	48.4	0.01248	17.81	0.8444	9.62 10^{-4}	51.73	0.9962

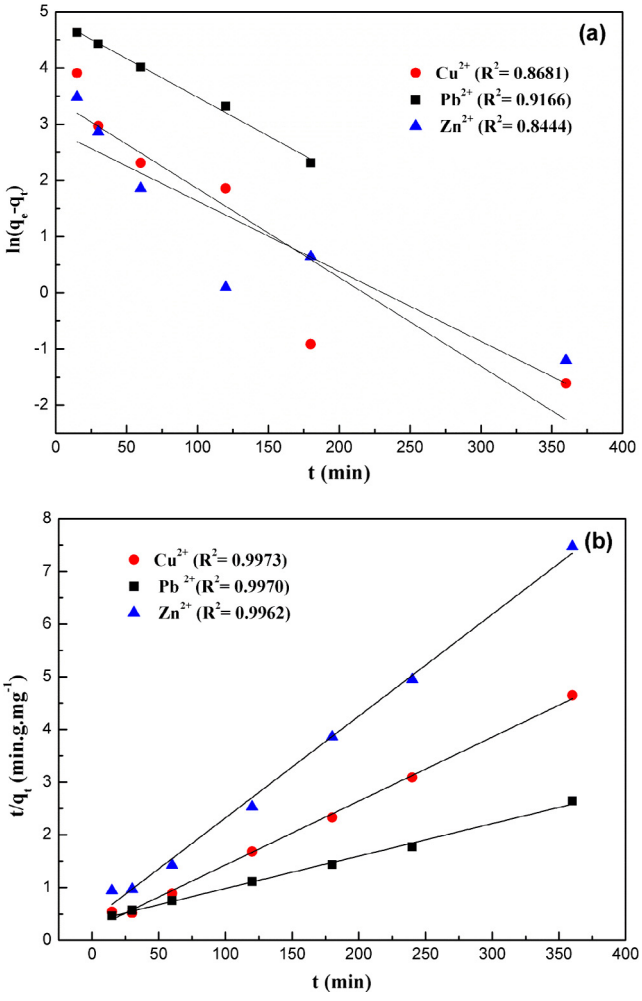

Figure 11 (a) Pseudo first-order kinetics and (b) second-order kinetics for metal ion adsorption onto MNP-Trz at 25 °C.

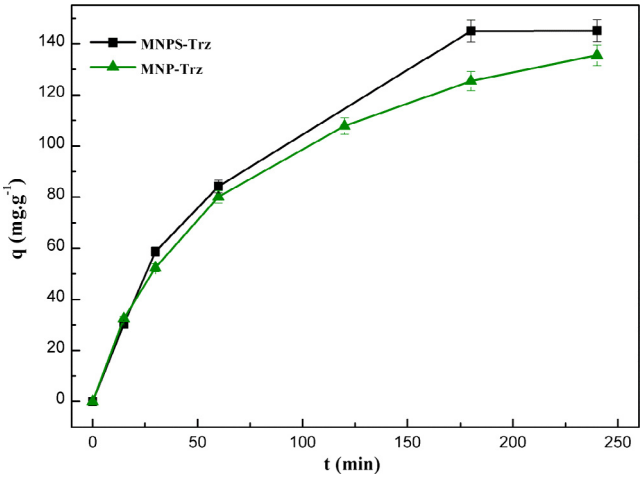

Figure 12 Effect of contact time on adsorption capacity of Pb (II) metal ion onto silica coated (MNPS-Trz) and uncoated (MNP-Trz) magnetic particles at 25 °C.

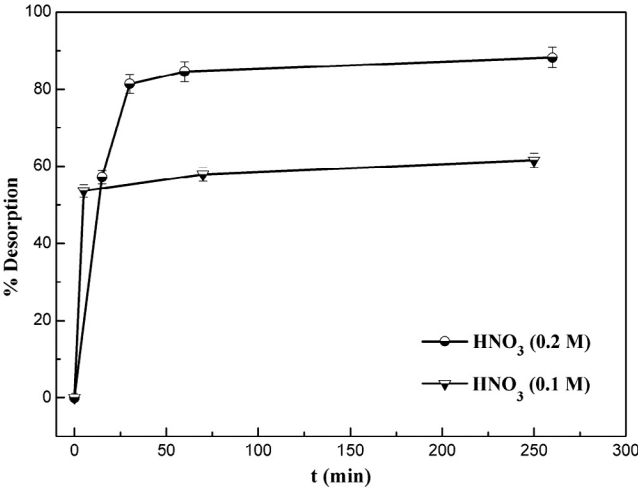

Figure 13 Effect of contact time in desorption efficiency of Pb (II) metal ion from the MNP-Trz adsorbent with different HNO_3 concentrations at T 25 °C.

0.2 mol L^{-1} HNO_3 within 30 min indicating a fast desorption process. The obtained results demonstrated that this magnetic solid support dispersion can be used efficiently for the removal and recovery of metal ions from wastewaters.

4. Conclusion

Novel functional colloidal dispersion adsorbents based on Fe_3O_4 magnetic nanoparticles bearing 1,2,3-triazole chelating units have been successfully prepared and characterized in this study. Immobilization of triazole unit onto magnetic core was chemically performed and confirmed by FTIR, TGA and Zeta potential analyses. The resulting particle colloidal particles show excellent magnetic performance and good dispersion in water. Cu^{2+}, Pb^{2+} and Zu^{2+} ions can be recovered efficiently from aqueous solution using these magnetic nano-adsorbents. The adsorption is highly pH-dependent and initial ion concentration. Maximum removal was observed at pH 5.5 and was achieved at 240 min. The adsorption kinetics followed the second order equation

for all studied systems suggesting that the rate-limiting step was chemical sorption. The adsorption equilibrium experimental results were well-fitted by the Langmuir isotherm model indicating monolayer adsorption mechanism.

The MNP-Trz material shows better adsorption performance than previously reported magnetic nano-adsorbents (Nassar, 2010; Li et al., 2012) with maximum adsorption capacities of 87.87, 167.78, and 51.20 mg g^{-1} for Cu^{2+}, Pb^{2+} and Zn^{2+} ions, respectively. Interestingly, high adsorption capacity in the case of Pb^{2+} was obtained for silica-coated homologous magnetic particles MNPS-Trz. The chemically inert silica layer protects magnetic core from chemical attacks and enhances the particles dispersibility in aqueous solution.

Results of this work suggest that the 1,2,3-triazole functionalized MNP should be a promising reusable adsorbents for removal of metal ions from wastewater effluents.

The outlined synthetic procedure can be tuned to introduce different functional groups into magnetic core *via* the addition of the relevant functionalized azide derivative to alkyne based magnetic nanoparticles. Further interactions with other pollutants such as organic dyes, pesticides or biomolecules can be considered for sensor and lab-on-a-chip applications.

Appendix A. Supplementary material

Supplementary data associated with this article can be found, in the online version, at http://dx.doi.org/10.1016/j.arabjc.2016.12.008.

References

Albarracín-Sánchez, J.L., Ureña-Amate, M.D., Socias-Viciana, M.M., Boutarbouch, N.D., 2013. Synthesis, characterization and adsorption properties of thermally activated hydrotalcites of varying Mg/Al ratio for the removal of nitrate from aqueous solution. J. Colloid Sci. Biotechnol. 2, 342–349. http://dx.doi.org/10.1166/jcsb.2013.1066.

Ambashta, R.D., Sillanpää, M., 2010. Water purification using magnetic assistance: a review. J. Hazard. Mater. 180, 38–49. http://dx.doi.org/10.1016/j.jhazmat.2010.04.105.

Badruddoza, A.Z.M., Hazel, G.S.S., Hidajat, K., Uddin, M.S., 2010. Synthesis of carboxymethyl-β-cyclodextrin conjugated magnetic nano-adsorbent for removal of methylene blue. Colloids Surf. Physicochem. Eng. Asp. 367, 85–95. http://dx.doi.org/10.1016/j.colsurfa.2010.06.018.

Badruddoza, A.Z.M., Tay, A.S.H., Tan, P.Y., Hidajat, K., Uddin, M.S., 2011. Carboxymethyl-β-cyclodextrin conjugated magnetic nanoparticles as nano-adsorbents for removal of copper ions: synthesis and adsorption studies. J. Hazard. Mater. 185, 1177–1186. http://dx.doi.org/10.1016/j.jhazmat.2010.10.029.

Banerjee, S.S., Chen, D.-H., 2007. Fast removal of copper ions by gum arabic modified magnetic nano-adsorbent. J. Hazard. Mater. 147, 792–799. http://dx.doi.org/10.1016/j.jhazmat.2007.01.079.

Broomberg, J., Gélinas, S., Finch, J.A., Xu, Z., 1999. Review of Magnetic Carrier Technologies for Metal Ion Removal. Magn. Electr. Sep 9, pp. 169–188, doi: 10.1155/1999/18035.

Calvo, B., Canoira, L., Morante, F., Martínez-Bedia, J.M., Vinagre, C., García-González, J.E., Elsen, J., Alcantara, R., 2009. Continuous elimination of Pb^{2+}, Cu^{2+}, Zn^{2+}, H^+ and NH_4^+ from acidic waters by ionic exchange on natural zeolites. J. Hazard. Mater. 166, 619–627. http://dx.doi.org/10.1016/j.jhazmat.2008.11.087.

Cao, H., He, J., Deng, L., Gao, X., 2009. Fabrication of cyclodextrin-functionalized superparamagnetic Fe3O4/amino-silane core–shell nanoparticles via layer-by-layer method. Appl. Surf. Sci. 255, 7974–7980. http://dx.doi.org/10.1016/j.apsusc.2009.04.199.

Caruntu, D., Caruntu, G., Chen, Y., O'Connor, C.J., Goloverda, G., Kolesnichenko, V.L., 2004. Synthesis of variable-sized nanocrystals of Fe_3O_4 with high surface reactivity. Chem. Mater. 16, 5527–5534. http://dx.doi.org/10.1021/cm0487977.

Chen, C., Hu, J., Shao, D., Li, J., Wang, X., 2009. Adsorption behavior of multiwall carbon nanotube/iron oxide magnetic composites for Ni(II) and Sr(II). J. Hazard. Mater. 164, 923–928. http://dx.doi.org/10.1016/j.jhazmat.2008.08.089.

Chen, G., 2004. Electrochemical technologies in wastewater treatment. Sep. Purif. Technol. 38, 11–41. http://dx.doi.org/10.1016/j.seppur.2003.10.006.

Crini, G., 2005. Recent developments in polysaccharide-based materials used as adsorbents in wastewater treatment. Prog. Polym. Sci. 30, 38–70. http://dx.doi.org/10.1016/j.progpolymsci.2004.11.002.

Crowley, J.D., Bandeen, P.H., 2009. A multicomponent CuAAC "click" approach to a library of hybrid polydentate 2-pyridyl-1,2,3-triazole ligands: new building blocks for the generation of metallosupramolecular architectures. Dalton Trans. 39, 612–623. http://dx.doi.org/10.1039/B911276F.

Duruibe, J.O.D., Ogwuegbu, M.O.C., Egwurugwu, J.N., 2007. Heavy metal pollution and human biotoxic effects. Int. J. Phys. Sci. 2, 112–118.

Feng, B., Hong, R.Y., Wang, L.S., Guo, L., Li, H.Z., Ding, J., Zheng, Y., Wei, D.G., 2008. Synthesis of Fe3O4/APTES/PEG diacid functionalized magnetic nanoparticles for MR imaging. Colloids Surf. Physicochem. Eng. Asp. 328, 52–59. http://dx.doi.org/10.1016/j.colsurfa.2008.06.024.

Fu, F., Wang, Q., 2011. Removal of heavy metal ions from wastewaters: a review. J. Environ. Manage. 92, 407–418. http://dx.doi.org/10.1016/j.jenvman.2010.11.011.

Ge, F., Li, M.-M., Ye, H., Zhao, B.-X., 2012. Effective removal of heavy metal ions Cd^{2+}, Zn^{2+}, Pb^{2+}, Cu^{2+} from aqueous solution by polymer-modified magnetic nanoparticles. J. Hazard. Mater. 211–212, 366–372. http://dx.doi.org/10.1016/j.jhazmat.2011.12.013.

Gurdeep, R., 2010. In: Adv. Inorgan. Chem., vol. Vol II. Madhya Chatwal, Meerut.

Hao, Y.-M., Man, C., Hu, Z.-B., 2010. Effective removal of Cu (II) ions from aqueous solution by amino-functionalized magnetic nanoparticles. J. Hazard. Mater. 184, 392–399. http://dx.doi.org/10.1016/j.jhazmat.2010.08.048.

Hu, H., Wang, Z., Pan, L., 2010. Synthesis of monodisperse Fe3O4@silica core–shell microspheres and their application for removal of heavy metal ions from water. J. Alloys. Compd. 492, 656–661. http://dx.doi.org/10.1016/j.jallcom.2009.11.204.

Huang, S.-H., Chen, D.-H., 2009. Rapid removal of heavy metal cations and anions from aqueous solutions by an amino-functionalized magnetic nano-adsorbent. J. Hazard. Mater. 163, 174–179. http://dx.doi.org/10.1016/j.jhazmat.2008.06.075.

Juríček, M., Kouwer, P.H.J., Rowan, A.E., 2011. Triazole: a unique building block for the construction of functional materials. Chem. Commun. 47, 8740–8749. http://dx.doi.org/10.1039/C1CC10685F.

Karatapanis, A.E., Fiamegos, Y., Stalikas, C.D., 2011. Silica-modified magnetic nanoparticles functionalized with cetylpyridinium bromide for the preconcentration of metals after complexation with 8-hydroxyquinoline. Talanta 84, 834–839. http://dx.doi.org/10.1016/j.talanta.2011.02.013.

Khan, S., Cao, Q., Zheng, Y.M., Huang, Y.Z., Zhu, Y.G., 2008. Health risks of heavy metals in contaminated soils and food crops irrigated with wastewater in Beijing, China. Environ. Pollut. 152, 686–692. http://dx.doi.org/10.1016/j.envpol.2007.06.056.

Lahmar, H., Saidi-Besbes, S., Elaissari, A., Derdour, A., 2015. Poly (1,2,3-triazole) latex particles: synthesis and chelating properties. J. Colloid Sci. Biotechnol. 4, 64–70. http://dx.doi.org/10.1166/jcsb.2015.1111.

Li, J., Zhang, S., Chen, C., Zhao, G., Yang, X., Li, J., Wang, X., 2012. Removal of Cu(II) and fulvic acid by graphene oxide nanosheets decorated with Fe_3O_4 nanoparticles. ACS Appl. Mater. Interf. 4, 4991–5000. http://dx.doi.org/10.1021/am301358b.

Mahdavian, A.R., Mirrahimi, M.A.-S., 2010. Efficient separation of heavy metal cations by anchoring polyacrylic acid on superpara-

magnetic magnetite nanoparticles through surface modification. Chem. Eng. J. 159, 264–271. http://dx.doi.org/10.1016/j.cej.2010.02.041.

Mohapatra, S., Mallick, S.K., Maiti, T.K., Ghosh, S.K., Pramanik, P., 2007. Synthesis of highly stable folic acid conjugated magnetite nanoparticles for targeting cancer cells. Nanotechnology 18, 385102. http://dx.doi.org/10.1088/0957-4484/18/38/385102.

Mohapatra, S., Pramanik, P., 2009. Synthesis and stability of functionalized iron oxide nanoparticles using organophosphorus coupling agents. Colloids Surf. Physicochem. Eng. Asp. 339, 35–42. http://dx.doi.org/10.1016/j.colsurfa.2009.01.009.

Nassar, N.N., 2010. Rapid removal and recovery of Pb(II) from wastewater by magnetic nanoadsorbents. J. Hazard. Mater. 184, 538–546. http://dx.doi.org/10.1016/j.jhazmat.2010.08.069.

Ngomsik, A.-F., Bee, A., Siaugue, J.-M., Talbot, D., Cubuil, V., 2009. Co(II) removal by magnetic alginate beads containing Cyanex 272®. J. Hazard. Mater. 166, 1043–1049. http://dx.doi.org/10.1016/j.jhazmat.2008.11.109.

Noelting, E., Michel, O., 1893. Direkte Ueberführung von Aminen in Diazoimide mittels Stickstoffwasserstoffsäure. Berichte. Dtsch. Chem. Ges. 26, 86–87. http://dx.doi.org/10.1002/cber.18930260119.

Obata, M., Kitamura, A., Mori, A., Kameyama, C., Czaplewska, J.A., Tanaka, R., Kinoshita, I., Kusumoto, T., Hashimoto, H., Harada, M., Mikata, Y., Funabiki, T., Yano, S., 2008. Syntheses, structural characterization and photophysical properties of 4-(2-pyridyl)-1,2,3-triazole rhenium(I) complexes. Dalton Trans. 25, 3292–3300. http://dx.doi.org/10.1039/B718538C.

Oliveira, L.C.A., Petkowicz, D.I., Smaniotto, A., Pergher, S.B.C., 2004. Magnetic zeolites: a new adsorbent for removal of metallic contaminants from water. Water Res. 38, 3699–3704. http://dx.doi.org/10.1016/j.watres.2004.06.008.

Ozaki, H., Sharma, K., Saktaywin, W., 2002. Performance of an ultra-low-pressure reverse osmosis membrane (ULPROM) for separating heavy metal: effects of interference parameters. Desalination 144, 287–294. http://dx.doi.org/10.1016/S0011-9164(02)00329-6.

Potgieter, J.H., Potgieter-Vermaak, S.S., Kalibantonga, P.D., 2006. Heavy metals removal from solution by palygorskite clay. Miner. Eng. 19, 463–470. http://dx.doi.org/10.1016/j.mineng.2005.07.004.

Ray, P.Z., Shipley, H.J., 2015. Inorganic nano-adsorbents for the removal of heavy metals and arsenic: a review. RSC. Adv. 5, 29885–29907. http://dx.doi.org/10.1039/C5RA02714D.

Rether, A., Schuster, M., 2003. Selective separation and recovery of heavy metal ions using water-soluble N-benzoylthiourea modified PAMAM polymers. React. Funct. Polym. 57, 13–21. http://dx.doi.org/10.1016/j.reactfunctpolym.2003.06.002.

Samiey, B., Cheng, C.-H., Wu, J., 2014. Organic-inorganic hybrid polymers as adsorbents for removal of heavy metal ions from solutions: a review. Materials 7, 673–726. http://dx.doi.org/10.3390/ma7020673.

Takafuji, M., Ide, S., Ihara, H., Xu, Z., 2004. Preparation of poly(1-vinylimidazole)-grafted magnetic nanoparticles and their application for removal of metal ions. Chem. Mater. 16, 1977–1983. http://dx.doi.org/10.1021/cm030334y.

Tran, H.V., Tran, L.D., Nguyen, T.N., 2010. Preparation of chitosan/magnetite composite beads and their application for removal of Pb(II) and Ni(II) from aqueous solution. Mater. Sci. Eng. C 30, 304–310. http://dx.doi.org/10.1016/j.msec.2009.11.008.

Tome, A.C., 2004. Product class 13: 1,2,3-triazole. In: Storr, R.C., Gilchrist, T.L. (Eds.), Science of Synthesis. Thieme, New York, pp. 415–601.

Wang, J., Zheng, S., Shao, Y., Liu, J., Xu, Z., Zhu, D., 2010. Amino-functionalized Fe3O4@SiO2 core–shell magnetic nanomaterial as a novel adsorbent for aqueous heavy metals removal. J. Colloid Int. Sci. 349, 293–299. http://dx.doi.org/10.1016/j.jcis.2010.05.010.

Xu, P., Zeng, G.M., Huang, D.L., Feng, C.L., Hu, S., Zhao, M.H., Lai, C., Wei, Z., Huang, C., Xie, G.X., Liu, Z.F., 2012. Use of iron oxide nanomaterials in wastewater treatment: a review. Sci. Total. Environ. 424, 1–10. http://dx.doi.org/10.1016/j.scitotenv.2012.02.023.

Xu, Z., Liu, Q., Finch, J.A., 1997. Silanation and stability of 3-aminopropyl triethoxy silane on nanosized superparamagnetic particles: I. Direct silanation. Appl. Surf. Sci. 120, 269–278. http://dx.doi.org/10.1016/S0169-4332(97)00234-1.

Yantasee, W., Warner, C.L., Sangvanich, T., Addleman, R.S., Carter, T.G., Wiacek, R.J., Fryxell, G.E., Timchalk, C., Warner, M.G., 2007. Removal of heavy metals from aqueous systems with thiol functionalized superparamagnetic nanoparticles. Environ. Sci. Technol. 41, 5114–5119. http://dx.doi.org/10.1021/es0705238.

Yacob, Z., Liebscher, J., 2015. Chemistry of 1,2,3-triazolium salts. In: Dehaen, W., Bakulev, V.A. (Eds.), Chemistry of 1,2,3-Triazoles. Springer, New York.

Zhang, X.-M., Zhao, Y.-F., Wu, H.-S., Batten, S.R., 2006. Syntheses and structures of metal tetrazole coordination polymers. Dalton Trans. 3170–3178. http://dx.doi.org/10.1039/B518052J.

Zhang, Y., Wang, X., Liu, J., Wu, L., 2013. Removal of copper (Cu^{2+}) from water using novel hybrid adsorbents: kinetics and isotherms. J. Chem. Eng. Data 58, 1141–1150. http://dx.doi.org/10.1021/je301168m.

Zhou, D., Zhang, L., Zhou, J., Guo, S., 2004. Cellulose/chitin beads for adsorption of heavy metals in aqueous solution. Water Res. 38, 2643–2650. http://dx.doi.org/10.1016/j.watres.2004.03.026.

Zhou, Y., Wang, S., Xie, Y., Guan, W., Ding, B., Yang, Z., Jiang, X., 2008. 1, 3-Dipolar cycloaddition as a general route for functionalization of Fe_3O_4 nanoparticles. Nanotechnology 19, 175601. http://dx.doi.org/10.1088/0957-4484/19/17/175601.

Zhu, Y., Hu, J., Wang, J., 2012. Competitive adsorption of Pb(II), Cu(II) and Zn(II) onto xanthate-modified magnetic chitosan. J. Hazard. Mater. 221–222, 155–161. http://dx.doi.org/10.1016/j.jhazmat.2012.04.026.